Absorption spectrum and gain without inversion of a driven two-level atom with arbitrary probe intensity in a squeezed vacuum

Peng Zhou[1] and S. Swain[1,2]
[1]*Department of Applied Mathematics and Theoretical Physics, The Queen's University of Belfast, Belfast BT7 1NN, United Kingdom*
[2]*Department of Physics, The University of Queensland, Brisbane, Queensland 4072, Australia*
(Received 8 April 1996)

We examine the response of a coherently driven two-level atom interacting with a broadband squeezed vacuum to a probe beam of arbitrary intensity. The equations of motion for the reduced density matrix elements are numerically solved by nonperturbative matrix inversion methods. For large driving intensities, the absorption spectrum exhibits a number of multiphoton absorption peaks with increasing probe strength in a standard vacuum and in a squeezed vacuum with small photon numbers, while the multiphoton absorption peaks are wiped out for large squeezed photon numbers. Strong gain without inversion at line center can be obtained in the presence of the squeezed vacuum when the probe strength does not exceed the driving one. The absorption spectrum is phase sensitive. We also find the presence of remarkable, very narrow structures at line center. In general, the spectrum is symmetric when $\Phi=0$ and π; otherwise, it is asymmetric and displays a dispersivelike profile at line center. [S1050-2947(97)02401-3]

PACS number(s): 42.50.Dv, 32.80.−t, 32.30.−r

I. INTRODUCTION

The absorption properties of driven atoms are of fundamental importance in techniques of high-resolution saturation spectroscopy. The absorption spectrum of a weak probe beam by a coherently driven two-level atom has been extensively studied theoretically, using linear response theory [1–5] and experimentally [6]. In the limit of a large driving field Rabi frequency, the spectrum has a three-peaked structure (the Mollow triplet) where the central peak has a Lorentzian line shape while the Rabi sidebands exhibit dispersionlike (Rayleigh-wing type) profiles [2,3]. However, when the driving field is detuned from resonance with the atomic transition frequency, the central resonance of the probe absorption spectrum exhibits a dispersionlike profile [3–5], while the sidebands are two Lorentzians in which one exhibits absorption and the other amplification. A physical interpretation of the dispersion profile at line center has been given in terms of interfering absorption pathways among dressed states by Grynberg and Cohen-Tannoudji [4]. Recently, Ling and Barbay, and Szymanowski *et al.* [5] have investigated the switching between the absorption and dispersion lineshapes of the probe absorption spectrum. They concluded that the Rabi sideband structures are due to coherently oscillating coherences while the central structures arise from the coherently oscillating populations. On the other hand, if the effect of rapid collisional dephasing is considered, the absorption spectrum for small Rabi frequencies exhibits a dip at line center [3], which is qualitatively different from that of the case of pure radiative damping. Again, the hole burning can be understood to originate from the coherent population oscillations which are induced by the pump and probe fields beating together at the difference frequency [3]. Lasing without inversion, operating on the three-photon sideband of the Mollow triplet, has also been investigated theoretically and experimentally [7].

If the probe strength increases, the atomic nonlinear response becomes substantial, and cannot be ignored. Consequently, the system exhibits a number of remarkable spectral features. Bonch-Bruevich *et al.* [8] observed the subradiative structures in the probe absorption spectrum, which are in agreement with theoretical results predicted by Toptygina and Fradkin [9]. Recently, Agarwal and Nayak, and Wilson-Gordon *et al.* [10] have investigated the effects of collisions and saturation on the higher-order nonlinear wave mixing processes, where multiphoton absorptions induced by both intense fields occur. Subharmonic resonances [11] and resonance fluorescence [12,13] of such a system have also been reported.

The successful generation of squeezed light has stimulated a re-examination of fundamental atomic radiative processes and the role of squeezed fluctuations in their interaction with atomic systems [14]. The first investigation by Gardiner [15] showed that the two quadratures of the polarization of a two-level atom interacting with a squeezed vacuum decay at vastly different rates, one being much enhanced and the other markedly diminished. It is the modification of the decays of the atomic dipole quadratures that gives rise to the unusual spectral features in the resonance fluorescence spectrum of a driven two-level atom in the squeezed vacuum, for instance, phase sensitivity of the linewidths and heights of the Mollow triplet [16], hole burning and dispersion profiles [17], and dark lines [18], which are qualitatively different from any predicted before for this system.

The effect of the squeezed vacuum on the weak probe beam absorption spectrum of a driven two-level atom has also been of considerable interest over the years. Ritsch and Zoller, and An *et al.* [19] have shown that for strong driving intensities, the absorption spectrum is phase sensitive and has subnatural linewidths, when both driving and squeezed fields are tuned to the atomic resonance. We have recently found that the anomalous spectral features, for example, pimples, hole burning, and dispersion profiles, at line center

of the probe absorption spectrum of such a system with intermediate Rabi intensities can take place in the vicinity of the critical point dividing the different dynamical regimes of the system, which marks the switch between probe absorption and amplification [20]. We have also studied squeezing-induced gain without inversion on resonance [21]. Ficek and Dalton [22] have recently considered the role of the detuning in the absorption spectrum of a two-level atom in the absence of a coherently driven field, in a Fabry-Pérot microcavity with injected squeezed light. An interesting phenomenon, squeezing-induced transparency, is obtained, which is qualitatively distinct from the one induced by the electromagnetic field in multilevel atomic systems [23]. We have recently found that probe transparency still occurs when the atom is coherently driven and the absorption spectrum exhibits Fano-like profiles in the large detuning and large squeezed photon number limit [24]. These remarkable results are also due to the influence of phase-sensitive field correlations on atomic dipole dynamics.

Previous studies concerning effects of a squeezed vacuum on the absorption spectra are subject to the condition that the probe field is sufficiently weak to leave the atomic evolution essentially unperturbed. In this paper we wish to study the absorption spectrum of the atom probed by a tunable field with an arbitrary intensity, which can induce the atomic polarization to oscillate at the frequency difference between the driving and probe fields and its harmonics, in the presence of a squeezed vacuum. We find that a rich variety of spectral profiles are possible. Particularly noteworthy results are as follows: (1) We find that remarkable structures—very narrow peaks within slightly broader dips— may occur for certain values of the parameters. The half-widths of these narrow peaks may be only 1–2% of the natural width. (2) Pronounced gain without population inversion is possible at line center, providing the probe beam intensity does not exceed the pump beam intensity.

Our paper is organized as follows. In Sec. II we solve the equations of motion of the reduced density matrix elements for a driven two-level atom illuminated by a probe field with an arbitrary strength in a squeezed vacuum, based on a nonperturbative infinite-dimensional matrix manipulation [13]. The numerical analysis of the probe absorption in such a system is presented in Sec. III. The final part contains a summary, and a brief discussion of the difficulties involved in experimentally investigating these effects.

II. EQUATIONS OF MOTION

The squeezed vacuum has been successfully generated in many laboratories using a parametric oscillator. Ideally, this is characterized by the correlation functions [14–22,24]

$$\langle a^{\dagger}(\omega)a(\omega')\rangle = N\delta(\omega-\omega'),$$

$$\langle a(\omega)a^{\dagger}(\omega')\rangle = (N+1)\,\delta(\omega-\omega'), \tag{1}$$

$$\langle a(\omega)a(\omega')\rangle = Me^{i\phi_s}\delta(2\omega_s-\omega-\omega'),$$

where $a(\omega)$ is the photon annihilation operator for the squeezed vacuum, ω_s is the center frequency of the squeezed vacuum (which is tuned close to the laser frequency ω_L), N is the squeezing photon number, M measures the strength of the two-photon correlations, and ϕ_s is the phase of the squeezed vacuum. The squeezing is assumed to be broadband so that N and M are independent of the frequency ω. They obey the following relation:

$$M=\eta\sqrt{N(N+1)} \quad (0\leqslant\eta\leqslant 1). \tag{2}$$

The value $\eta=1$ indicates an ideal squeezed vacuum, i.e., one that shows the maximum degree of squeezing possible for a given N, while $\eta=0$ corresponds to no squeezing at all — a chaotic field. The squeezed vacuum may be ''turned off'' by setting $N=0$.

We here consider the interaction of such a squeezed vacuum with a two-level atom driven by a monochromatic laser field of frequency ω_L with amplitude $\mathbf{E}_L$, and simultaneously illuminated by a tunable probe field of frequency ω_p with amplitude $\mathbf{E}_p$. For simplicity, we assume that both field modes have the same phase ϕ. The equations of motion for the reduced atomic density matrix elements, in the rotating-wave approximation, take the form (in units of $\hbar$)

$$\begin{aligned}
\dot{\rho}_{10} &= -(\Gamma+i\omega_A)\rho_{10}-\gamma Me^{-i(2\omega_s t-\phi_s)}\rho_{01}+i\tfrac{1}{2}\Omega[e^{-i(\omega_L t-\phi)} \\
&\quad +\alpha e^{-i(\omega_p t-\phi)}]\rho_z, \\
\dot{\rho}_z &= -2\Gamma\rho_z+i\Omega[e^{i(\omega_L t-\phi)}+\alpha e^{i(\omega_p t-\phi)}]\rho_{10} \\
&\quad -i\Omega[e^{-i(\omega_L t-\phi)}+\alpha e^{-i(\omega_p t-\phi)}]\rho_{01}-\gamma,
\end{aligned} \tag{3}$$

$$\rho_{01}=\rho_{10}^{*},$$

$$\rho_z=\rho_{11}-\rho_{00},$$

with

$$\Omega=2\mu_{10}E_L, \quad \alpha=\frac{E_p}{E_L}, \quad \Gamma=\gamma(N+\tfrac{1}{2}), \tag{4}$$

where Ω is the Rabi frequency of the driving field, α is the ratio of the probe amplitude to the driving one, which may assume arbitrary values, μ_{10} is the dipole moment of the atomic transition, and γ is the spontaneous decay rate of the atom to the normal vacuum,

Previous studies of such a system concentrated mostly on very weak probe intensities, $\alpha\ll 1$, where the atomic nonlinear responses to the probe field are negligible [19–21, 24], so that the induced atomic polarization oscillates at three dominant frequencies, ω_L, ω_p, and $2\omega_L-\omega_p$. The latter reflects the fact that a four-wave-mixing signal, which is associated with a three-photon process consisting of a two-photon absorption of the driving field and a one-photon emission of the weak probe beam, is generated. However, for arbitrary probe intensities, both driving and probe fields, in general, induce components of the atomic polarization oscillating not only at

frequencies ω_L and ω_p, but at the frequencies $n\omega_L \pm m\omega_p$ as well, where n and m are integers. Therefore, we may expand $\rho_{10}(t), \rho_{01}(t)$, and $\rho_z(t)$ in the Fourier series

$$\rho_{10}(t)=\sum_{n=-\infty}^{+\infty}\rho_{10}(\omega_L-n\delta)e^{-i[(\omega_L-n\delta)t-\phi]}$$
$$=e^{-i(\omega_L t-\phi)}\sum_{n=-\infty}^{+\infty}X_1^{(n)}e^{in\delta t},$$
$$\rho_{01}(t)=\sum_{n=-\infty}^{+\infty}\rho_{01}(\omega_L+n\delta)e^{i[(\omega_L+n\delta)t-\phi]}$$
$$=e^{i(\omega_L t-\phi)}\sum_{n=-\infty}^{+\infty}X_2^{(n)}e^{in\delta t}, \tag{5}$$
$$\rho_z(t)=\sum_{n=-\infty}^{+\infty}\rho_z(n\delta)e^{in\delta t}=\sum_{n=-\infty}^{+\infty}X_3^{(n)}e^{in\delta t},$$

where $\delta=\omega_p-\omega_L$ is the frequency difference between the driving and probe fields, a continuously tunable quantity.

Substituting Eq. (5) into Eq. (3) leads to

$$\dot{X}_1^{(n)}=-(\Gamma+i\Delta+in\delta)X_1^{(n)}-\xi^*X_2^{(n)}$$
$$+i\tfrac{1}{2}\Omega[X_3^{(n)}+\alpha X_3^{(n+1)}],$$
$$\dot{X}_2^{(n)}=-(\Gamma-i\Delta+in\delta)X_2^{(n)}-\xi X_1^{(n)}-i\tfrac{1}{2}\Omega[X_3^{(n)}+\alpha X_3^{(n-1)}], \tag{6}$$
$$\dot{X}_3^{(n)}=-(2\Gamma+in\delta)X_3^{(n)}-\gamma\delta_{n,0}+i\Omega[X_1^{(n)}+\alpha X_1^{(n-1)}]$$
$$-i\Omega[X_2^{(n)}+\alpha X_2^{(n+1)}],$$

where $\Delta=\omega_A-\omega_L$ is a detuning of the driving field from the atomic transition frequency, $\xi=\gamma M e^{i\Phi}$ where $\Phi=2\phi-\phi_s$ is the relative phase between the squeezed vacuum and the fields.

From the definition Eq. (5), one sees that $X_1^{(0)}=\rho_{10}(\omega_L)$, $X_1^{(-1)}=\rho_{10}(\omega_p)$, $X_1^{(1)}=\rho_{10}(2\omega_L-\omega_p)$, ..., and $X_1^{(n)}=\rho_{10}[(n+1)\omega_L-n\omega_p]$, where, as we shall see in the next section, $\rho_{10}(\omega_L)$ and $\rho_{10}(\omega_p)$ are associated with atomic complex polarizations that yield refractive index and absorption (or amplification) characteristics for the driving and probe modes, respectively, while $\rho_{10}(2\omega_L-\omega_p)$ represents a four-wave-mixing response, which gives rise to generation of an optical wave with frequency $2\omega_L-\omega_p$, and so on. However, $X_3^{(0)}=\rho_z(0)$ indicates the dc component of the atomic population inversion, while $X_3^{(\pm n)}=\rho_z(\pm n\delta)$ represents the population pulsations oscillating at harmonics of the beat frequency between the pump and probe fields.

In the steady state the Fourier amplitudes are independent of time, i.e., $\dot{X}_k^{(n)}=0$. From Eq. (6) the steady-state amplitudes are of the form

$$X_1^{(n)}=\frac{i(\Omega/2)[(\Gamma_n-i\Delta+\xi^*)X_3^{(n)}+\alpha(\Gamma_n-i\Delta)X_3^{(n+1)}+\alpha\xi^*X_3^{(n-1)}]}{\Gamma_n^2+\Delta^2-|\xi|^2},$$
$$X_2^{(n)}=\frac{-i(\Omega/2)[(\Gamma_n+i\Delta+\xi)X_3^{(n)}+\alpha(\Gamma_n+i\Delta)X_3^{(n-1)}+\alpha\xi X_3^{(n+1)}]}{\Gamma_n^2+\Delta^2-|\xi|^2}, \tag{7}$$

where $X_3^{(n)}$ is a solution of the recurrence relation

$$A_nX_3^{(n)}+B_nX_3^{(n-1)}+C_nX_3^{(n+1)}+D_nX_3^{(n-2)}$$
$$+E_nX_3^{(n+2)}=-\gamma\delta_{n,0} \tag{8}$$

with

$$A_n=(\Gamma+\Gamma_n)+\frac{\Omega^2}{2}\left(\frac{2\Gamma_n+\xi+\xi^*}{\Gamma_n^2+\Delta^2-|\xi|^2}+\alpha^2\frac{\Gamma_{n-1}-i\Delta}{\Gamma_{n-1}^2+\Delta^2-|\xi|^2}\right.$$
$$\left.+\alpha^2\frac{\Gamma_{n+1}+i\Delta}{\Gamma_{n+1}^2+\Delta^2-|\xi|^2}\right),$$
$$B_n=\frac{\Omega^2}{2}\alpha\left(\frac{\Gamma_n+i\Delta+\xi^*}{\Gamma_n^2+\Delta^2-|\xi|^2}+\frac{\Gamma_{n-1}-i\Delta+\xi^*}{\Gamma_{n-1}^2+\Delta^2-|\xi|^2}\right),$$
$$C_n=\frac{\Omega^2}{2}\alpha\left(\frac{\Gamma_n-i\Delta+\xi}{\Gamma_n^2+\Delta^2-|\xi|^2}+\frac{\Gamma_{n+1}+i\Delta+\xi}{\Gamma_{n+1}^2+\Delta^2-|\xi|^2}\right), \tag{9}$$
$$D_n=\frac{\Omega^2}{2}\alpha^2\frac{\xi^*}{\Gamma_{n-1}^2+\Delta^2-|\xi|^2},$$
$$E_n=\frac{\Omega^2}{2}\alpha^2\frac{\xi}{\Gamma_{n+1}^2+\Delta^2-|\xi|^2}$$

where $\Gamma_n=\Gamma+in\delta$. Clearly, if there is no squeezing, $D_n=0$ and $E_n=0$, and the quantity $X_3^{(n)}$ couples only to $X_3^{(n-1)}$ and $X_3^{(n+1)}$.

In order to solve the recurrence relation Eq. (8), using matrix inversion methods recently proposed by Ficek and Freedhoff [13], we construct an infinite-dimensional column vector $\mathbf{X}_3$ by putting together the amplitudes $X_3^{(n)}$ in the order

$$\mathbf{X}_3=\begin{bmatrix}\vdots\\ X_3^{(-1)}\\ X_3^{(0)}\\ X_3^{(1)}\\ \vdots\end{bmatrix}. \tag{10}$$

The recurrence Eq. (8) can then be solved in the form

$$\mathbf{X}_3 = \underline{\overline{K}}^{-1}\mathbf{G}, \tag{11}$$

where K is an infinite-dimensional matrix composed of the coefficients A_n, B_n, C_n, D_n, E_n,

$$\underline{\overline{K}} = \begin{bmatrix} & \cdots & & & & & \\ B_{-2} & A_{-2} & C_{-2} & E_{-2} & & 0 & \\ D_{-1} & B_{-1} & A_{-1} & C_{-1} & E_{-1} & & \\ & D_0 & B_0 & A_0 & C_0 & E_0 & \\ & & D_1 & B_1 & A_1 & C_1 & E_1 \\ & 0 & & D_2 & B_2 & A_2 & C_2 \\ & & & & & \cdots & \end{bmatrix} \tag{12}$$

and $\mathbf{G}$ is an infinite-dimensional vector

$$\mathbf{G} = \begin{bmatrix} \vdots \\ 0 \\ -\gamma \\ 0 \\ \vdots \end{bmatrix}. \tag{13}$$

The solution (11), together with Eq. (7), can be used to obtain the atomic dynamics to any desired accuracy simply by matrix inversion. To invert the matrix K we truncate the dimension of the vector $\mathbf{X}_3$ at a large number n of terms. For given parameters Ω, α, Δ, and δ, we choose the number n to be sufficiently large for us to achieve the same accuracy for $X_3^{(n_0)}$ when we increase or reduce n by one. All our numerical calculations of the probe absorption below are based on these exact solutions.

III. PROBE ABSORPTION SPECTRUM

For simplicity, we assume that the system is composed of an ensemble of identical and independent driven two-level atoms, so that the polarization of the medium is determined by the expectation value of the dipole operator multiplied by the density of the atoms [3]. Therefore, the polarization can be related to the off-diagonal elements of the atomic density matrix

$$P(t) = \mathcal{N}\mu_{10}\left(\sum_{n=-\infty}^{+\infty} \rho_{10}(\omega_L - n\delta) e^{-i[(\omega_L - n\delta)t - \phi]} + \text{c.c.} \right), \tag{14}$$

which harmonically oscillate at the frequencies of the driving and probe fields, and combinations of both field frequencies. $\mathcal{N}$ is the number density of atoms. We are here interested in the response of the medium to the probe field, which can be expressed as

$$P_{\text{probe}}(t) = \epsilon_0 E_p [\chi(\omega_p) e^{-i(\omega_p t - \phi)} + \text{c.c.}], \tag{15}$$

where ϵ_0 is the free space permittivity and $\chi(\omega_p)$ the susceptibility whose real and imaginary parts contribute to the refractive index and absorption coefficient, respectively.

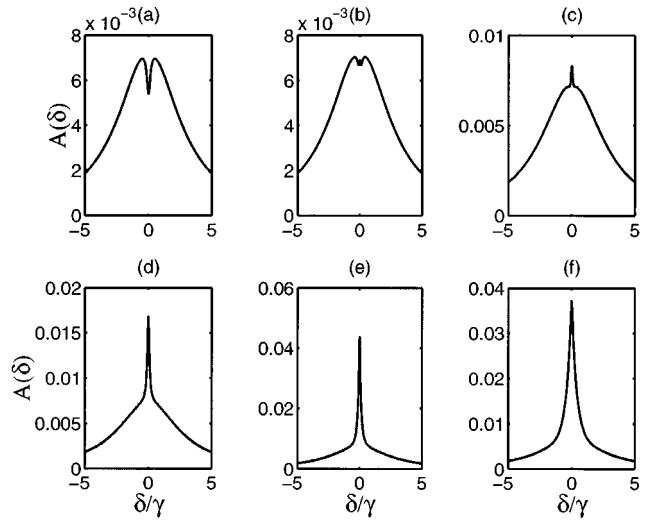

FIG. 1. The dimensionless absorption spectrum for the probe beam as a function of $\delta = (\omega_p - \omega_L)$, for the squeezed photon number $N = 1$ and phase $\Phi = 0$ and the Rabi frequency $\Omega = 0.5$, with different probe intensities, (a) $\alpha = 0.00001$, (b) $\alpha = 0.18$, (c) $\alpha = 0.25$, (d) $\alpha = 0.5$, (e) $\alpha = 1$, and (f) $\alpha = 3$, respectively. (We take $\Delta = 0, \eta = 1$, and $\gamma = 1$ throughout these figures.)

Comparing Eqs. (14) with (15), the susceptibility $\chi(\omega_p)$ at the probe field frequency ω_p may be expressed in terms of the off-diagonal elements of the density matrix $\rho_{10}(\omega_p)$

$$\chi(\omega_p) = \frac{\mathcal{N}\mu_{10}}{\epsilon_0 E_p} \rho_{10}(\omega_p). \tag{16}$$

Therefore, the renormalized probe absorption spectrum may be defined as

$$A(\omega_p) = \frac{\Omega}{\alpha} \text{Im}[\rho_{10}(\omega_p)] = \frac{\Omega}{\alpha} \text{Im}[X_1^{(-1)}], \tag{17}$$

where $X_1^{(-1)}$ is determined by Eq. (7).

We now discuss the numerical results. In Figs. 1–10 we assume $\Phi = 0$. The effect of varying the squeezing phase is shown in Fig. 11. Figure 1 presents the probe absorption spectra for the squeezed photon number $N = 1$ and phase $\Phi = 0$ and a weak driving strength ($\Omega = 0.5$) for values of the probe field strength increasing from $\alpha = 10^{-5}$ in the first frame to $\alpha = 3$ in the final frame. When the probe field is sufficiently weak, for example, in Fig. 1(a) where $\alpha = 10^{-5}$, the spectrum reduces to that found using linear response theory [20], where squeezing-induced hole burning occurs at line center. As the probe intensity increases, the hole burning becomes shallower, and eventually an additional narrow resonance takes place at the center of the dip. This may just be seen in the frame 1(b) where $\alpha = 0.18$. In frame 1(c), where α has been increased to $\alpha = 0.25$, the hole-burning is replaced by a sharp peak. It should be borne in mind that, in the absence of the squeezed vacuum, $N = 0$, the spectrum consists of a single, Lorentzian-like peak at line center with half-width of the order of γ, for the whole range of values of α. The squeezed vacuum is entirely responsible for the remarkable very narrow features at line center.

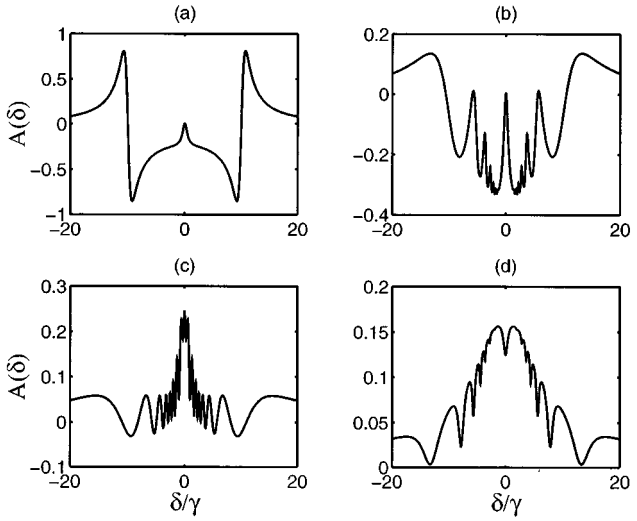

FIG. 2. Same as Fig. 1, but for $N=0$, $\Omega=10$, and (a) $\alpha=0.00001$, (b) $\alpha=0.5$, (c) $\alpha=1$, and (d) $\alpha=2$.

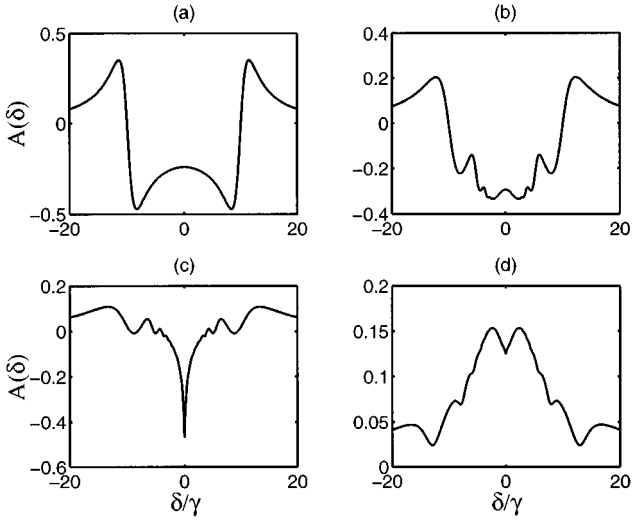

FIG. 3. Same as Fig. 2, but for $N=1$.

As the probe strength continues to increase, the narrow central peak gains in intensity. The central resonance is dominant and non-Lorentzian when the probe strength is comparable with the driving intensity, as we illustrate in the frames 1(d)–1(f), where $\alpha=0.5$, 1, and 3, respectively. These frames also show that the central peak for the cases $\alpha\lesssim 1$ is much narrower than for the cases of $\alpha\gg 1$.

We investigate numerically the behavior of the probe absorption for large Rabi frequencies ($\Omega=10\gamma$) with different probe intensities α in Figs. 2–4. In Fig. 2 we first consider the case of the standard vacuum, $N=0$. The probe absorption spectra are far more interesting for the large Rabi frequency case than for the $\Omega=0.5$ case. The spectra in the standard vacuum exhibit an increasing number of multiphoton absorption peaks within the frequency region $-\Omega\leqslant\delta\leqslant\Omega$ as the probe field intensity increases, up to the value $\alpha=1$, as illustrated in Fig. 2(c), after which the number of peaks decreases again, as we see for $\alpha=2$ in Fig. 2(d).

When a weak to moderate squeezed vacuum is present, up to $N\simeq 1$, the major effect is that the difference between the peaks and dips in the wings of the spectrum diminishes, while the central portion becomes depressed. We show these features in Fig. 3, where the parameters are taken the same as Fig. 2, except $N=1$. One can also see that for the larger Rabi frequencies, strong amplification in the central regions is possible with the assistance of the squeezed vacuum, at least for $\alpha\leqslant 1$. Interestingly, there are regions away from line center where gain is possible even for $\alpha=1$. Thus energy may be absorbed from a beam of equal intensity. For the larger values of α [Fig. 3(d)], no gain is possible for any value of δ, and we obtain just a dip at line center.

The spectral profiles are diverse for differing probe intensities. When $\alpha=1$, which means that both fields have the same intensity, all the sidebands are dispersivelike. See, for example, Figs. 2(c) and 3(c). However, for $\alpha<1$, e.g., Figs. 2(b) and 3(b), the outermost sidebands exhibit dispersivelike profiles while the others are absorptivelike; and for $\alpha>1$, e.g., Figs. 2(d) and 3(d), the absorptivelike peaks are replaced by diplike profiles.

For larger values of N, such as $N=5$ in Fig. 4, the multiphoton absorption peaks are wiped out, but the amplification remains at line center for $\alpha\leqslant 1$. The amplification region is broad for small α, but deep and narrow for $\alpha=1$. However, for $\alpha=2$ in the frame 4(d) we actually obtain a small, very sharp peak at line center. This peak has a width of the order of a tenth of the natural linewidth. Remarkably, if we amplify the region around this peak, we find that it has structure: there is actually a very narrow hole bored in the center of this peak with a half-width of the order of 5% of γ.

It is worth emphasizing that the amplification of the probe beam at the atomic transition frequency ω_A when the probe strength does not exceed the driving one is due to squeezing, but there is no population inversion. (We have examined the population inversion and found it to be negative, though this is not displayed here.)

In Fig. 5 we examine the amplification at line center from a different point of view by plotting $A(0)$ against α for $\Omega=10$ and $N=0$, 0.1,1, and 10 in frames 5(b), 5(c), and 5(d), respectively. We see that the central value of the spec-

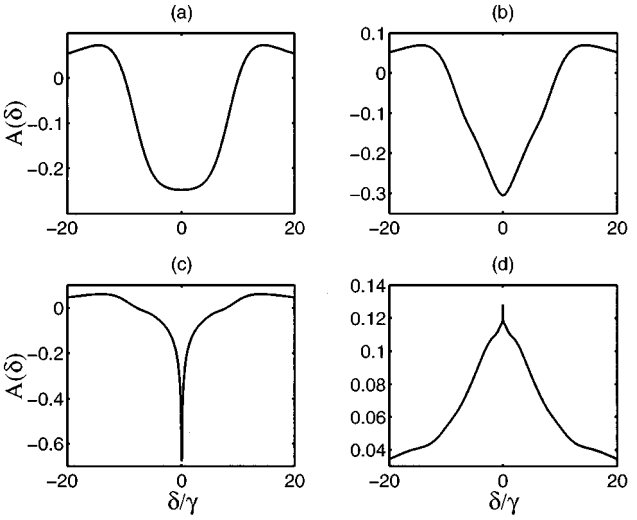

FIG. 4. Same as Fig. 2, but for $N=5$.

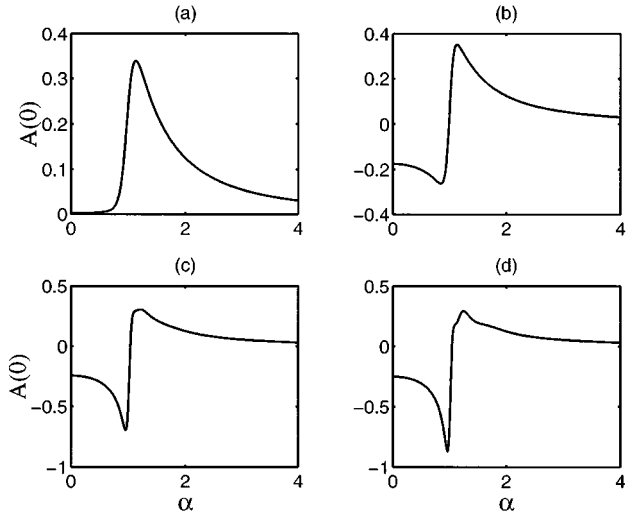

FIG. 5. The central value of the dimensionless probe absorption spectrum as a function of α, for the Rabi frequency $\Omega=10$, the squeezed phase $\Phi=0$, and different squeezed photon numbers, (a) $N=0$ (a standard vacuum), (b) $N=0.1$, (c) $N=1$,(d) $N=10$.

trum varies dramatically with α in the neighborhood of $\alpha=1$. The final three frames show once more that, in a squeezed vacuum, gain at line center is possible when $\alpha\lesssim 1$, that the gain reaches a maximum value for α close to 1, and then switches to absorption for a value of α slightly greater than 1. The larger the squeezed photon number, the larger the maximal gain obtained. The probe does not gain energy from the pump beam at line center when its intensity slightly exceeds that of the pump beam.

Not only does the amplification vary rapidly near $\alpha=1$, but so does the whole spectral profile. This is illustrated in Fig. 6 where $\Omega=10$, $N=1$, and $\alpha=1,1.025,1.05$, and 1.1. We see the development of a very sharp spike at line center as α increases. Thus, while amplification is possible at line

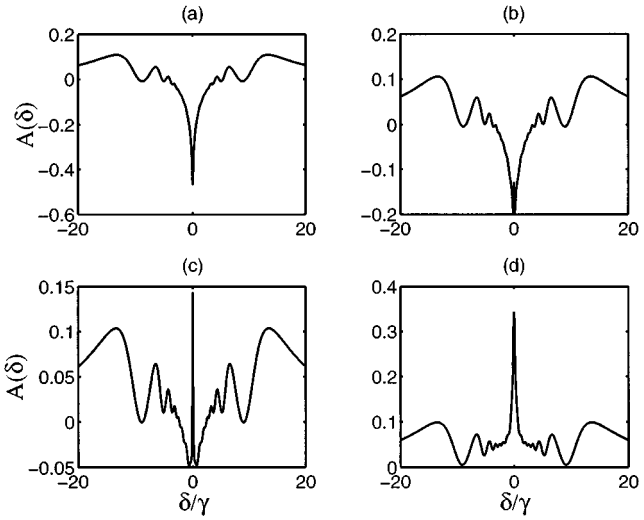

FIG. 6. The dimensionless absorption spectrum for the probe intensity close to the driving intensity, i.e., $\alpha=1$, for the Rabi frequency $\Omega=10$, the squeezed phase $\Phi=0$, and the squeezed photon numbers $N=1$: (a) $\alpha=1$, (b) $\alpha=1.025$, (c) $\alpha=1.05$, (d) $\alpha=1.1$.

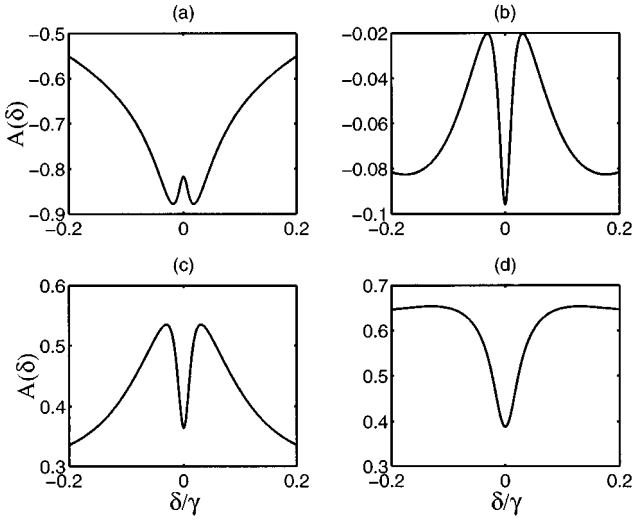

FIG. 7. The central region of the dimensionless probe absorption spectrum for the Rabi frequency $\Omega=50$, the squeezed phase $\Phi=0$, and the squeezed photon number $N=1$, with (a) $\alpha=1$, (b) $\alpha=1.025$, (c) $\alpha=1.05$, (d) $\alpha=1.1$.

center for $\alpha=1.025$, the sharp spike prevents this at $\alpha=1.05$, although amplification is still possible for other frequencies. For $\alpha=1.1$, as shown in frame 6(d), there is no amplification at any frequency. The central sharp line in frame 6(c) is noteworthy, its width being only a few percent of the natural linewidth.

The sharp features at line center in the above figures surprisingly show further structure when magnified. They possess an even sharper central dip for the case of a maximum, or a small sharp peak in the case of a minimum. This is shown in Fig. 7, where we magnify the central regions by a factor of 100. We have actually increased Ω to $\Omega=50$ in order to make the structure more apparent, but the features are qualitatively similar in the $\Omega=10$ case considered in Fig. 6. The central dip in frame 7(b), for example, has a half-width of only 1% of γ. The width of these features increases quite rapidly with α.

Figure 8 indicates the variation of the spectral profiles of the probe absorption with the squeezed photon number for the case $\alpha=1$ and $\Omega=5$. It demonstrates clearly the tendency of the central peak to be depressed in the presence of the squeezed vacuum. It is evident that the sidebands disappear and the central component exhibits increasing gain of the probe beam as the photon number N increases. On the other hand, the larger the value of N, the narrower the frequency domain of gain without population inversion.

The variation of the spectral profiles with Rabi frequency for $N=\alpha=1$ is shown in Fig. 9, which demonstrates, first, the radical differences in behavior between weak and strong probes and, second, that increasing the Rabi frequency gives rise to an increased number of sidebands, associated with multiphoton processes. We find that Figs. 1(b) and 9(b) have a similar spectral structure: very sharp features occurring at the center of the dip. However, Figs. 1 and 9 represent two contrasting tendencies of spectral evolution. The former exhibits that the dip at line center is elevated with increasing probe intensity (for fixed driving intensity), while the latter

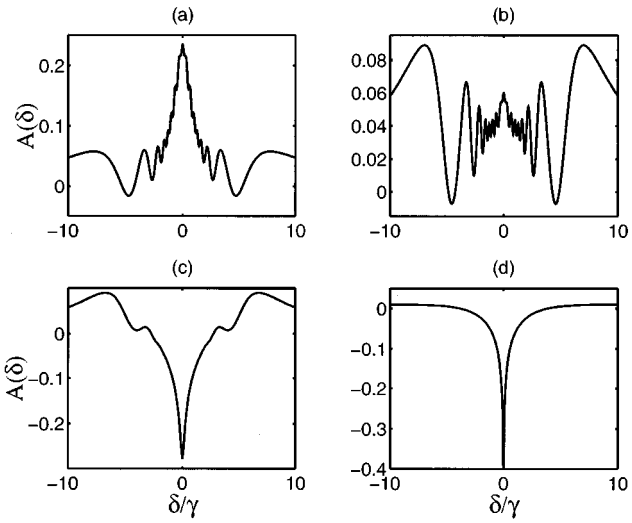

FIG. 8. Same as Fig. 1, but for $\Omega=5$, $\alpha=1$, and $\Phi=0$, with various squeezed photon numbers, (a) $N=0$, (b) $N=0.1$, (c) $N=1$, and (d) $N=10$.

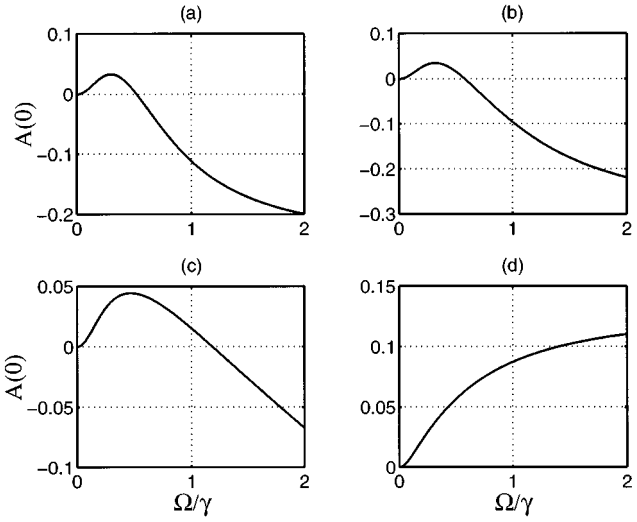

FIG. 10. The central value of the dimensionless probe absorption spectrum as a function of Ω/γ, for $N=1$, $\Phi=0$, and different probe intensities, (a) $\alpha=0.00001$, (b) $\alpha=0.5$, (c) $\alpha=1$, and (d) $\alpha=2$.

demonstrates that the central peak is depressed as the intensities of both the probe and driving fields increase proportionally.

Figure 9 also implies the existence of a threshold value of the Rabi frequency that marks the change from probe absorption to amplification at line center. When the Rabi frequency is less than this value, the atom will absorb the probe beam, while it will amplify the probe beam when the Rabi frequency is larger than this value. In order to display this in detail, we plot the central value of the absorption spectrum versus the Rabi frequency in Fig. 10. One can see that the threshold value, corresponding to $A(0)=0$, i.e., probe transparency, increases as the probe intensity increases. However, this threshold does not exist when the probe intensity sufficiently exceeds the driving intensity. For $\alpha>1+\varepsilon(N,\Omega)$, where ε is small, it is impossible to amplify the probe beam at line center for any Rabi frequency. However, as we have indicated previously, a small amount of amplification may be possible at certain frequencies away from line center if α does not greatly exceed unity.

So far we have displayed results only for the case $\Phi=0$. Figure 11 shows the variation of the absorption spectrum with the phase, for the case $\Omega=10$, $N=\alpha=1$. One sees that when $\Phi=0$, the π spectrum is symmetric; otherwise, it is asymmetric, with a dispersivelike profile at line center being exhibited. We progress from a central minimum to a central maximum as Φ increases. For the case $\Phi=\pi$, probe gain never occurs.

IV. SUMMARY

In this paper we have solved the equations of motion of a driven two-level atom probed by a frequency-tunable field

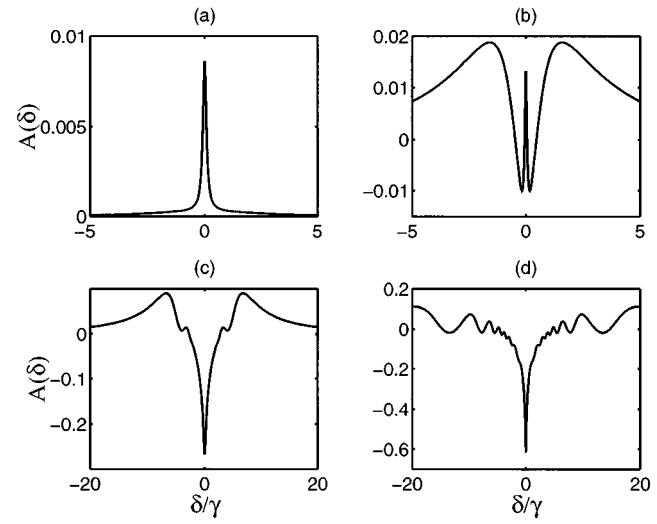

FIG. 9. Same as Fig. 1, but for $\alpha=1$, $N=1$, and $\Phi=0$, with various Rabi frequencies, (a) $\Omega=0.1$, (b) $\Omega=1$, (c) $\Omega=5$, and (d) $\Omega=15$.

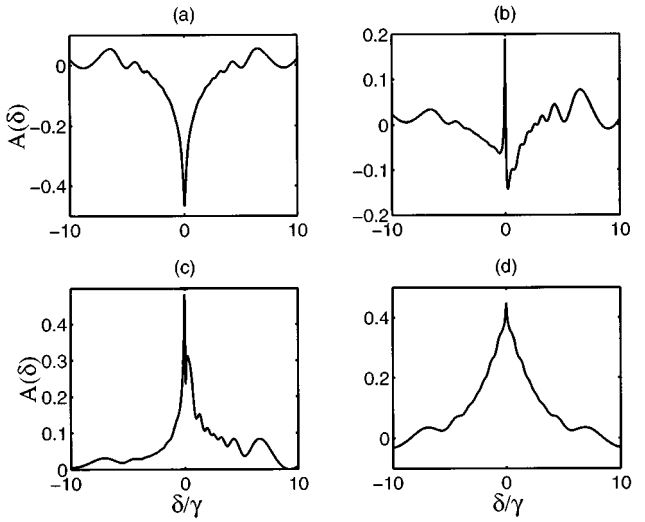

FIG. 11. Same as Fig. 1, but for $\Omega=10$, $\alpha=1$, and $N=1$, with different squeezed phases, (a) $\Phi=0$, (b) $\Phi=\pi/4$, (c) $\Phi=\pi/2$, and (d) $\Phi=\pi$.

with arbitrary intensity in the presence of a squeezed vacuum. The absorption spectrum for the probe beam is examined numerically. For very weak probe field strength the absorption spectrum is in agreement with those obtained by linear response theory, where the spectrum has the Mollow triplet structure, and the sidebands exhibit dispersivelike profiles in the strong driving field (which is tuned to atomic resonance). As the probe strength increases, the spectrum exhibits a number of multiphoton resonances for small squeezed photon numbers, while the multiphoton processes are wiped out for large squeezed photon numbers. The spectral features are strongly dependent on the probe intensity. When both field strengths are the same, all the sidebands display dispersivelike profiles. However, when the probe intensity is less than the driving one, the outermost sidebands are dispersivelike and the others show absorptivelike profiles, while the absorptivelike features are replaced by diplike profiles when the probe intensity is larger than the driving one.

For some ranges of the parameters, we have shown the existence of remarkably sharp features at line center, which show even sharper structure, with half-widths of about 1% of the natural linewidth.

Gain without inversion at line center has been shown to occur in the presence of the squeezed vacuum when the probe intensity does not greatly exceed the driving one. Gain is most pronounced for $\Phi = 0$ and does not occur for $\Phi = \pi$. The absorption spectrum is phase sensitive, being symmetric when the squeezing phase satisfies $\Phi = 0$ and $\Phi = \pi$. Otherwise, the spectrum is asymmetric and dispersive profiles at line center may be obtained.

It is worth pointing out that these effects would be difficult to realize experimentally in the free-space situation considered here since they require *all* the vacuum modes with which the atom interacts to be squeezed [15,16]. That is, the squeezed modes must occupy the whole 4π solid angle of space. On the other hand, experiments need a small window of unsqueezed vacuum modes in order to view the fluorescence from the atom. Therefore, experiments manifesting the effect of squeezed light on the atomic radiative properties would probably require some sort of cavity system, where the atom interacts strongly only with the privileged cavity mode, so that only the modes within a small solid angle about the cavity mode need be squeezed. Recently, theoretical studies have shown that the anomalous spectral features, brought about by the squeezed vacuum, in the resonance fluorescence and the absorption of a weak probe beam can be carried over to the cavity situation in the bad cavity limit [25], but with reduced magnitudes. However, they still remain detectable within the cavity environment. This does indicate that the effects reported here may occur in a cavity configuration, which may be a practical scenario for experimentally investigating the modifications of the atomic radiative properties by squeezed light.

ACKNOWLEDGMENTS

This work is supported by the United Kingdom EPSRC, by the EC, and by a NATO Collaborative Research Grant. We would like to thank Dr. B. J. Dalton, Dr. Z. Ficek, and Dr. T. A. B. Kennedy for helpful conversations. P.Z. wishes to thank the Queen's University of Belfast for financial support.

[1] B. R. Mollow, Phys. Rev. A **5**, 2217 (1972).
[2] G. S. Agarwal, Phys. Rev. A **19**, 923 (1979).
[3] M. Sargent III, Phys. Rep. **43**, 223 (1978); R. W. Boyd, M. G. Raymer, P. Narum, and D. J. Harter, Phys. Rev. A **24**, 411 (1981); P. Meystre and M. Sargent III, *Elements of Quantum Optics* (Springer-Verlag, Berlin, 1991).
[4] G. Grynberg and C. Cohen-Tannoudji, Opt. Commun. **96**, 150 (1993).
[5] H. Y. Ling and S. Barbay, Opt. Commun. **111**, 350 (1994); C. Szymanowski, C. H. Keitel, B. J. Dalton, and P. L. Knight, J. Mod. Opt. **42**, 985 (1995).
[6] F. Y. Wu, S. Ezekiel, M. Ducloy, and B. R. Mollow, Phys. Rev. Lett. **38**, 1077 (1977).
[7] D. Grandclement, G. Gryberg, and M. Pinard, Phys. Rev. Lett. **59**, 40 (1987); **59**, 44 (1987); G. S. Agarwal, Opt. Commun., **80**, 37 (1990); J. Zakrzewski, Phys. Rev. A **46**, 6010 (1992).
[8] A. M. Bonch-Bruevich, T. A. Vartanyan, and N. A. Chigir, Zh. Éksp. Teor. Fiz. **77**, 1899 (1979) [Sov. Phys. JETP **50**, 901 (1979)]; A. M. Bonch-Bruevich, S. G. Przhibelskii, and N. A. Chigir, *ibid.* **80**, 565 (1981) [*ibid.* **53**, 285 (1981)].
[9] G. I. Toptygina and E. E. Fradkin, Sov. Phys. JETP **55**, 246 (1982).
[10] G. S. Agarwal and N. Nayak, J. Opt. Soc. Am. B **1**, 164 (1984); Phys. Rev. A **33**, 391 (1986); A. D. Wilson-Gordon and H. Friedmann, *ibid*. **36**, 1333 (1987); **38**, 4087 (1988).
[11] S. Chakmahijan, K. Koch, and C. R. Stroud, Jr., J. Opt. Soc. Am. B **5**, 2015 (1988); K. Koch, B. J. Oliver, S. Chakmahijan, and C. R. Stroud, Jr., *ibid.* **6**, 58 (1989); W. M. Ruyten, *ibid*. **6**, 1796 (1989); **9**, 1892 (1992).
[12] Y. Zhu, Q. Wu, A. Lezama, D. J. Gauthier, and T. W. Mosserg, Phys. Rev. A **41**, R6574 (1990); S. P. Tewari and M. K. Kumari, *ibid*. **41**, R5273 (1990); H. S. Freedhoff and Z. Chen, *ibid*. **41**, 6013 (1990); **46**, 7328(E) (1992); G. S. Agarwal, Y. Zhu, D. J. Gauthier, and T. W. Mosserg, J. Opt. Soc. Am. B **8**, 1163 (1991).
[13] Z. Ficek and H. S. Freedhoff, Phys. Rev. A **48**, 3092 (1993).
[14] H. J. Carmichael, in *Atomic and Molcular Physica and Quantum Optics*, edited by H. A. Bachor, K. Kumar, and B. A. Robson (World Scientific, Singapore, 1992); A. S. Parkins, in *Modern Nonlear Optics, Part 2*, edited by M. Evans and S. Kielich (Wiley, New York, 1993).
[15] C. W. Gardiner, Phys. Rev. Lett. **56**, 1917 (1986).
[16] H. J. Carmichael, A. S. Lane, and D. F. Walls, Phys. Rev. Lett. **58**, 2539 (1987); J. Mod. Opt. **34**, 821 (1987).
[17] S. Smart and S. Swain, Phys. Rev. A **48**, R50 (1993); S. Swain, Phys. Rev. Lett. **73**, 1493 (1994); S. Swain and P. Zhou, Phys. Rev. A **52**, 4845 (1995).
[18] J. M. Courty and S. Reynaud, Europhys. Lett. **10**, 237 (1989); C. Cabrillo, W. S. Smyth, S. Swain, and P. Zhou, Opt. Commun. **114**, 344 (1995).

[19] H. Ritsch and P. Zoller, Opt. Commun. **64**, 523 (1987); **66**, 333(E) (1988); Phys. Rev. A **38**, 4657 (1988); S. An, M. Sargent III, and D. F. Walls, Opt. Commun. **67**, 373 (1988); S. An and M. Sargent III, Phys. Rev. A **39**, 3998 (1989).

[20] P. Zhou, Z. Ficek, and S. Swain, J. Opt. Soc. Am. B **13**, 768 (1996).

[21] Z. Ficek, W. S. Smyth, and S. Swain, Opt. Commun. **110**, 555 (1994); Phys. Rev. A **52**, 4126 (1995).

[22] Z. Ficek and B. J. Dalton, Opt. Commun. **102**, 231 (1993).

[23] S. E. Harris, J. E. Field, and A. Imamoglu, Phys. Rev. Lett. **64**, 1107 (1990); K. Hakuta, L. Marmet, and B. P. Stoicheff, Phys. Rev. A **45**, 5152 (1992); M. Xiao, Y. Li, S. Jin, and J. Gea-Banacloche, Phys. Rev. Lett. **74**, 666 (1995).

[24] P. Zhou and S. Swain, Quantum Semiclass. Opt. **8**, 959 (1996).

[25] P. S. Rice and L. M. Pedrotti, J. Opt. Soc. Am. B **9**, 2008 (1992); W. S. Smyth and S. Swain, Phys. Rev. A **53**, 2846 (1996); P. Zhou and S. Swain, Opt. Commun. **131**, 153 (1996).